AGU PUBLICATIONS

Geophysical Research Letters

RESEARCH LETTER
10.1002/2016GL070649

Key Points:
- An updated land surface model predicts a trend of +0.2%/yr in global wetland CH_4 emissions over 1993-2014, mainly driven by temperature
- An atmospheric model using these wetland fluxes, along with other emission estimates, agrees well with ground-based and satellite CH_4 data
- Varying global wetland CH_4 emissions (±3%) made a small contribution to the 1999-2006 pause but contributed ~1 ppb/yr to growth post-2006

Supporting Information:
- Supporting Information S1

Correspondence to:
J. McNorton,
j.r.mcnorton@leeds.ac.uk

Citation:
McNorton, J., E. Gloor, C. Wilson, G. D. Hayman, N. Gedney, E. Comyn-Platt, T. Marthews, R. J. Parker, H. Boesch, and M. P. Chipperfield (2016), Role of regional wetland emissions in atmospheric methane variability, *Geophys. Res. Lett.*, *43*, 11,433–11,444, doi:10.1002/2016GL070649.

Received 29 JUL 2016
Accepted 15 OCT 2016
Accepted article online 19 OCT 2016
Published online 12 NOV 2016

Role of regional wetland emissions in atmospheric methane variability

J. McNorton[1,2], E. Gloor[3], C. Wilson[1,2], G. D. Hayman[4], N. Gedney[5], E. Comyn-Platt[4], T. Marthews[4], R. J. Parker[6,7], H. Boesch[6,7], and M. P. Chipperfield[1,2]

[1]School of Earth and Environment, University of Leeds, Leeds, UK, [2]National Centre for Earth Observation, University of Leeds, Leeds, UK, [3]School of Geography, University of Leeds, Leeds, UK, [4]Centre for Ecology and Hydrology, Wallingford, UK, [5]Met Office Hadley Centre, Joint Centre for Hydro-Meteorological Research, Wallingford, UK, [6]Earth Observation Science Group, Department of Physics and Astronomy, University of Leicester, Leicester, UK, [7]National Centre for Earth Observation, University of Leicester, Leicester, UK

Abstract Atmospheric methane (CH_4) accounts for ~20% of the total direct anthropogenic radiative forcing by long-lived greenhouse gases. Surface observations show a pause (1999–2006) followed by a resumption in CH_4 growth, which remain largely unexplained. Using a land surface model, we estimate wetland CH_4 emissions from 1993 to 2014 and study the regional contributions to changes in atmospheric CH_4. Atmospheric model simulations using these emissions, together with other sources, compare well with surface and satellite CH_4 data. Modeled global wetland emissions vary by ±3%/yr ($\sigma = 4.8$ Tg), mainly due to precipitation-induced changes in wetland area, but the integrated effect makes only a small contribution to the pause in CH_4 growth from 1999 to 2006. Increasing temperature, which increases wetland area, drives a long-term trend in wetland CH_4 emissions of +0.2%/yr (1999 to 2014). The increased growth post-2006 was partly caused by increased wetland emissions (+3%), mainly from Tropical Asia, Southern Africa, and Australia.

1. Introduction

Two outstanding features of the recent global atmospheric CH_4 record are as follows: (i) prior to 2007 atmospheric CH_4 seemed to be approaching a stationary state with sources and sinks in balance and (ii) since 2007 growth has resumed [*Rigby et al.*, 2008]. The reasons for these two features are not fully understood, but several indicators suggest that changes in wetlands contributed to both. First, wetland emissions are the largest single source of CH_4 to the atmosphere (~175 Tg/yr, 30% of total) and are known to be sensitive to climate variation. Thus, interannual variations will have an effect at the global scale [*Bousquet et al.*, 2006; *Ciais et al.*, 2014] and may produce a positive climate feedback in the future [*Gedney et al.*, 2004; *Melton et al.*, 2013]. Second, the isotopic signature of atmospheric CH_4 has become more depleted in $^{13}CH_4$ since 2007, which may be explained by a shift toward a larger fraction of biogenic sources, i.e., wetlands [*Nisbet et al.*, 2014], or agricultural sources [*Schaefer et al.*, 2016]. However, both of these studies focused on the global isotopic signature of CH_4 and so were unable to spatially resolve the regions of main CH_4 emission changes.

Previous investigations into wetland CH_4 emissions using land surface models (LSMs) have shown large differences between estimates, both in magnitude and the spatial and temporal distribution [*Wania et al.*, 2010; *Riley et al.*, 2011; *Kirschke et al.*, 2013; *Melton et al.*, 2013]. Most of these studies were not evaluated against observations of atmospheric CH_4 concentrations, in particular recent column observations [*Wunch et al.*, 2011; *Parker et al.*, 2015]. Studies using atmospheric models forced by a combination of modeled wetland emissions and nonwetland source estimates were not fully consistent with both in situ and space-based CH_4 measurements [e.g., *Patra et al.*, 2011; *Fraser et al.*, 2013; *Hayman et al.*, 2014]. *Meng et al.* [2015] showed good agreement between surface measurements and model simulations when using a wetland CH_4 model, but they did not include emissions after 2005. This was, in part, due to a reliance on the Global Inundation Extent from Multi-Satellites product for estimated wetland area extent and time variation, which only covers the period from 1993 to 2007 [*Prigent et al.*, 2012]. It is therefore preferable to have an emission model that is able to predict wetland extent accurately and independently of observational data.

Building on the work of *Hayman et al.* [2014], we have further developed the Joint UK Land Environment Simulator (JULES) and used it to simulate CH_4 emissions from 1993 to 2014. Important updates to the wetland

model include improved representation of topography, which provides a more realistic spatial extent and temporal evolution of flooded areas [*Marthews et al*., 2015], and inclusion of dynamic soil carbon pools [*Clark et al*., 2011]. We first compare our modeled wetland CH_4 emissions with a top-down estimate available for 2003–2011 [*Bloom et al*., 2012]. We then combine the derived wetland CH_4 emissions with nonwetland emission estimates for use in an atmospheric chemical transport model (CTM), TOMCAT, and compare the simulated concentrations to long-term ground-based observations. We have taken advantage, for the first time, of the ~5 year atmospheric column CH_4 measurements from the Greenhouse gases Observing SATellite (GOSAT) remote sensing mission [*Parker et al*., 2011, 2015] to further evaluate the model. We demonstrate good agreement with both satellite-derived and surface CH_4 data, which allows us to investigate the role of wetland emissions in atmospheric CH_4 variability.

2. Methods

2.1. Wetland Flux Models

Wetlands are areas where the soil is saturated, either permanently or seasonally [*Melton et al*., 2013]. Within anaerobic wetland regions methanogenesis occurs [e.g., *Christensen et al*., 2003]. This CH_4 production process is primarily dependent on available substrate and soil temperature. Additional processes, which influence emissions, have been included in other LSMs [e.g., *Wania et al*., 2010; *Riley et al*., 2011]. We evaluated the importance of these within JULES by comparing simulations against surface flux observations and found that their inclusion currently provides either limited or no improvement on model performance (see supporting information) [*Gauci et al*., 2004; *Turnock et al*., 2015]. These comparisons highlight uncertainties in wetland emissions at a site-specific scale ($R = 0.32$). Therefore, due to process uncertainties, our analysis considers only temperature, wetland area, and organic substrate as controls of wetland CH_4 emissions.

We use JULES v3.4.1 [*Clark et al*., 2011] to derive spatially and temporally resolved global wetland CH_4 emissions from 1993 to 2014 (hereafter labelled JU). The model was forced by 3-hourly WATCH-forcing-data-ERA-interim (WFDEI) at a horizontal resolution of $0.5° \times 0.5°$ [*Weedon et al*., 2014]. The rainfall component of WFDEI was bias corrected using Global Precipitation Climatology Centre (GPCC) and Climatic Research Unit measurements. Wetland fraction derivations were based on an improved topographic index within the JULES-TOPography-based hydrological MODEL, which produces significant improvements compared with previous versions [*Marthews et al*., 2015]. The topographic index and water table depth, which is controlled by precipitation, evaporation, and runoff, are the key controls of wetland area. For the wetland CH_4 flux estimation, equation (1) in *Gedney et al*. [2004] was updated to use the four carbon pools generated as part of both the RothC model [*Jenkinson et al*., 1990; *Coleman and Jenkinson*, 1999] and the Top-down Representation of Interactive Foliage and Flora Including Dynamics [*Cox*, 2001] model within JULES. The updated flux model is as follows:

$$f_{sub} = C_{dpm}R_{dpm} + C_{rpm}R_{rpm} + C_{bio}R_{bio} + C_{hum}R_{hum} \quad (1)$$

$$F_{CH_4} = k_{CH_4} f_{wet} f_{sub} Q_{10} (T_{soil})^{(T_{soil}-T_0)/10} \quad (2)$$

The total temperature independent methanogenesis (f_{sub}, in kg m^{-2} s^{-1}) is based on the four carbon pools of decomposable plant material (C_{dpm}, kg m^{-2}), resistant plant material (C_{rpm}), biomass (C_{bio}), and long-lived humus (C_{hum}), which are multiplied by their respective methanogenesis rates ($R_{dpm/rpm/bio/hum}$, s^{-1}). These rates used to calculate a CH_4 flux (F_{CH_4}, kg m^{-2} s^{-1}) are assumed to be the same as the respiration rates used in *Clark et al*. [2011] (see supporting information). The soil temperature (T_{soil}, K) is averaged over the top 10 cm, and the reference temperature (T_0) is 273.15 K. At temperatures below 273.15 K the ground is considered frozen with zero surface flux. An effective Q_{10} value, based on the reaction rate change for a 10 K change in temperature, was initially set at 3, based on *McNorton et al*. [2016a], and varies with temperature between 2.5 and 3 as given by equation (2) in *Gedney et al*. [2004]. The wetland fraction (f_{wet}) is the fraction of the model grid cell area that is water saturated. A unitless constant (k_{CH_4}) was calibrated to provide mean global emissions of 175 Tg/yr between 2000 and 2009, based on *Ciais et al*. [2014].

First, we use top-down CH_4 emission data derived using the method of *Bloom et al*. [2012] (hereafter labelled BL) to evaluate JU. BL is based on column CH_4 (XCH_4) retrievals from the Scanning Imaging Absorption Spectrometer for Atmospheric Chartography, gravity anomaly-derived equivalent water height

from the Gravity Recovery and Climate Experiment, proxy soil temperature from the National Centers for Environmental Prediction/National Center for Atmospheric Research skin temperature analyses, and an assumed surface carbon input. This data set provides interannually varying emissions between 2003 and 2011; a climatology is used for 1993–2002 and 2012–2014. BL emissions, combined with nonwetland emissions, have previously been shown to compare well with observed surface concentrations when used as a boundary condition in an atmospheric CTM [*Bloom et al*., 2012]. We therefore use them as a benchmark for JU for the period 2003–2011. JU is suitable for the study of long-term trends because it is not limited by availability of satellite data. As with JU, we scaled BL to provide mean global emissions of 175 Tg/yr between 2000 and 2009.

2.2. Atmospheric CH_4 Model

We used the TOMCAT global atmospheric 3-D off-line CTM [*Chipperfield*, 2006] to predict atmospheric CH_4 concentrations given surface emissions. We performed three simulations, two of which used interannually varying wetlands (TOMCAT-JU and TOMCAT-BL) and the third used a climatology of JULES emissions between 1993 and 2014 (TOMCAT-CL). Simulations were forced by the 6-hourly European Centre for Medium-Range Weather Forecasts ERA-Interim reanalyses [*Dee et al*., 2011] for the period 1993 to 2014 with a horizontal resolution of $2.8° \times 2.8°$ and 60 levels from the surface to ~60 km. The model was spun-up from 1977 to 1992 using interannually varying emissions when available; these include JULES wetland fluxes then the mean global CH_4 was rescaled to match observed concentrations in 1993.

Anthropogenic emissions were taken from the EDGAR v4.2 FT 2010 database, which gradually increase between 1993 and 2010, with 2011–2014 emissions set to repeat 2010 [*Olivier et al*., 2012]. Previous studies have suggested a range of overestimates in the growth rate in EDGAR anthropogenic emissions [*Bousquet et al*., 2011; *Monteil et al*., 2011; *Patra et al*., 2016]. The magnitude of the overestimated growth is highly uncertain; as an estimate, we reduced the growth rate between 2000 and 2010 by a factor of 2. Biomass burning emissions were taken from the GFED v4 database [*van der Werf et al*., 2010] between 1997 and 2014, with 1993–1996 emissions based on a climatology. Annually repeating hydrate, mud volcano, and termite and ocean [*Matthews and Fung*, 1987] emissions were taken from the TransCom CH_4 study [*Patra et al*., 2011]. JULES only simulates natural wetlands and does not account for agricultural practices (e.g., fertilization) altering the biogeochemical processes. To account for rice paddies in areas of natural wetlands, a mask (based on the MICRA2000 rice fraction map) [*Portmann et al*., 2010] was placed over the JU and BL wetlands and annual repeating emissions [*Yan et al*., 2009] were used instead. Any climate-driven influences on rice emissions are not accounted for. All nonwetland emissions are scaled to 2000–2009 values provided by *Ciais et al*. [2014] (see supporting information).

Removal of atmospheric CH_4 follows *Patra et al*. [2011], where loss occurs through chemical reactions with OH, Cl, $O(^1D)$, and a soil sink. We use the same model OH fields as *McNorton et al*. [2016b]. These are a development of fields used by *Patra et al*. [2011], which were derived from a combination of semiempirically calculated tropospheric distributions and 2-D model stratospheric values [*Spivakovsky et al*., 2000; *Huijnen et al*., 2010]. We use CH_3CCl_3 anomalies to vary the model OH field interannually between 1997 and 2007 [*Montzka et al*., 2011; *McNorton et al*., 2016b]. For the other years the original *Patra et al*. [2011] field is used. The Cl, $O(^1D)$, and soil sink fields do not vary interannually.

2.3. Satellite CH_4 Data

We use the University of Leicester Proxy dry air column-averaged mole fractions of CH_4 (XCH_4) v6.0 data [*Parker et al*., 2011, 2015] derived from observations made by the TANSO-FTS instrument on board the GOSAT satellite [*Kuze et al*., 2009]. Retrievals of XCH_4 are sensitive to the surface and lower troposphere, hence providing information relating to emissions of CH_4. GOSAT has provided global XCH_4 data since 2009 with a single-sounding precision between 0.4 and 0.8%, making it an ideal tool for the assessment of modeled atmospheric CH_4.

To compare TOMCAT to GOSAT, we take the nearest model profile, both spatially and temporally, to the GOSAT retrieval. We also apply the sounding-specific GOSAT averaging kernel to the model profile to account for the differing sensitivities throughout the atmosphere, allowing the most robust comparison between measurement and model. Both GOSAT and model output are then binned into TransCom regions and temporally into monthly periods between 2009 and 2014.

2.4. Ground-Based CH_4 Observations

We use atmospheric CH_4 measurements from the Total Carbon Column Observing Network (TCCON) (see supporting information) [*Wunch et al*., 2011] and the National Oceanic and Atmospheric Administration/Earth System Research Laboratory (NOAA/ESRL) sampling sites [*Dlugokencky et al*., 2015]. These allow us to assess the model's ability to reproduce the observed long-term trends in CH_4 growth. To derive global surface CH_4 concentrations, we have used observations from 19 NOAA sites [see *McNorton et al*., 2016b, Table 1] interpolated across 180 latitude bins, which were then weighted by surface area. The process was repeated for model output sampled at the site locations.

3. Results and Discussion

Figure 1 compares the JU and BL emissions globally and for defined TransCom regions [see *Gurney et al*., 2002]. Annual emissions from JU compare well with BL in most regions although JU emissions tend to be noticeably higher in tropical regions and lower in boreal regions, caused in part by JU ($Q_{10}(T_0) = 3$) having a higher temperature sensitivity than BL ($Q_{10}(T_0) = 1.65$). Methanogenesis temperature sensitivity varies depending on conditions; as a result there is uncertainty when assuming a global value [*Segers*, 1998]. For the time period when both predictions are available (2003–2011), global annual emissions range from 169.4 Tg/yr (2004) to 183.1 Tg/yr (2010) in JU and from 172.1 Tg/yr (2004) to 178.6 Tg/yr (2007) in BL. The mean interannual variability is larger in JU (4.1 Tg/yr) than in BL (2.0 Tg/yr). Both data sets show an overall positive trend in global emissions over their respective time periods, statistically significant at the 95% level ($p < 0.05$), of 0.37 Tg/yr for JU (1993–2014) and 0.55 Tg/yr for BL (2003–2011). Nearly all of the growth trends in JU originate from Europe (0.07 Tg/yr), Tropical Asia (0.13 Tg/yr), Southern Africa (0.05 Tg/yr), and Australia (0.10 Tg/yr), whereas trends in BL are largest from Eurasian Boreal (0.11 Tg/yr), Northern Africa (0.10 Tg/yr), and Southern Africa (0.13 Tg/yr). The spatial difference in trends occurs not only as a result of model differences but also as a result of the time periods covered by each model. When emissions are divided into the time periods before, during, and after the observed CH_4 pause, there appears to be no noticeable decrease in JU emissions during the pause (Figure 1b). However, modeled emissions are typically slightly above average early in the pause period (1999–2001, 179.9 Tg/yr) and smaller in the later pause period (2002–2006, 171.5 Tg/yr), indicating that changes in wetland emissions were not responsible for the initial stall in CH_4 growth but may have contributed later on.

Figure 2a shows that the variability in JU CH_4 emissions is larger in tropical than in boreal regions, with anomalously high tropical emissions between 2007 and 2012, offset by lower emissions between 2002 and 2006. Figure 2b shows positive long-term trends in JU wetland CH_4 emissions over Southeast Asia, northern Australia, Zambia, southern Democratic Republic of Congo, and the seasonally flooded savannas in tropical South America. Distinct regions with negative trends are less apparent, with the exception of the Iberá wetlands (Paraná river, NE, Argentina).

Variability in wetland fraction, soil temperature, and carbon substrate is the cause of trends in our modeled JU wetland CH_4 emissions. We investigated anomalies in these parameters both zonally (Figures 3a, 3c, and 3d) and globally (Figure 3e). Considerable wetland area anomalies occur at both boreal and tropical latitude bands, with an anomalously low tropical wetland area during both the 1997/1998 El Niño event and the later period of the pause in growth (2002–2006) and anomalously high post-2006. Figures 3b and 3f show interannual variability in wetland area that occurs as a result of changes in the reanalysis rainfall over wetland regions [*Harris et al*., 2014; *Weedon et al*., 2014].

Soil temperature anomalies in wetland regions predicted by JULES are heavily weighted toward the tropics (Figure 3c), whereas carbon substrate flux anomalies are weighted toward the northern boreal regions (Figure 3d). Our results show positive Northern Hemisphere tropical wetland temperature anomalies during the 1997/1998 El Niño event and in 2010. Negative tropical wetland temperature anomalies are found early in the simulation from 1993 to 2001 (excluding 1997/1998).

To further investigate these trends, we calculated grid cell coefficient anomalies, which are based on the flux as a function of each variable, to satisfy the following rewrite of equation (2):

$$F_{CH_4} = k_{CH_4} \cdot f_{tem} \cdot f_{wet} \cdot f_{sub} \quad (3)$$

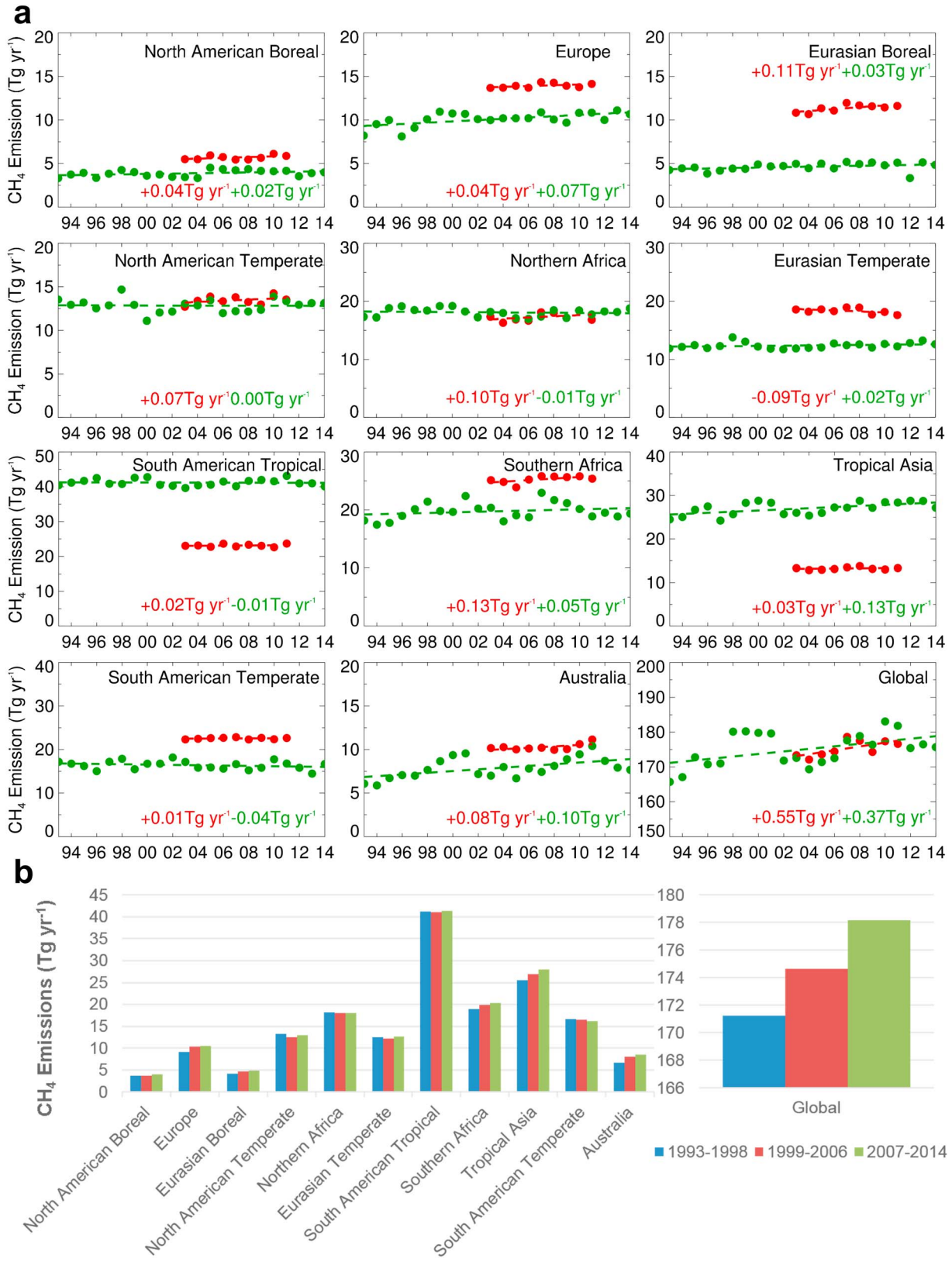

Figure 1. (a) Annual CH_4 wetland emissions (Tg/yr) from JU (green, 1993–2014) and BL (red, 2003–2011) data sets. Panels show 11 TransCom regions and the global total. Annotated values are linear regression emission trends for JU (1993–2014) and BL (2003–2011). (b) Mean annual regional and global JU emissions averaged between 1993–1998, 1999–2006, and 2007–2014.

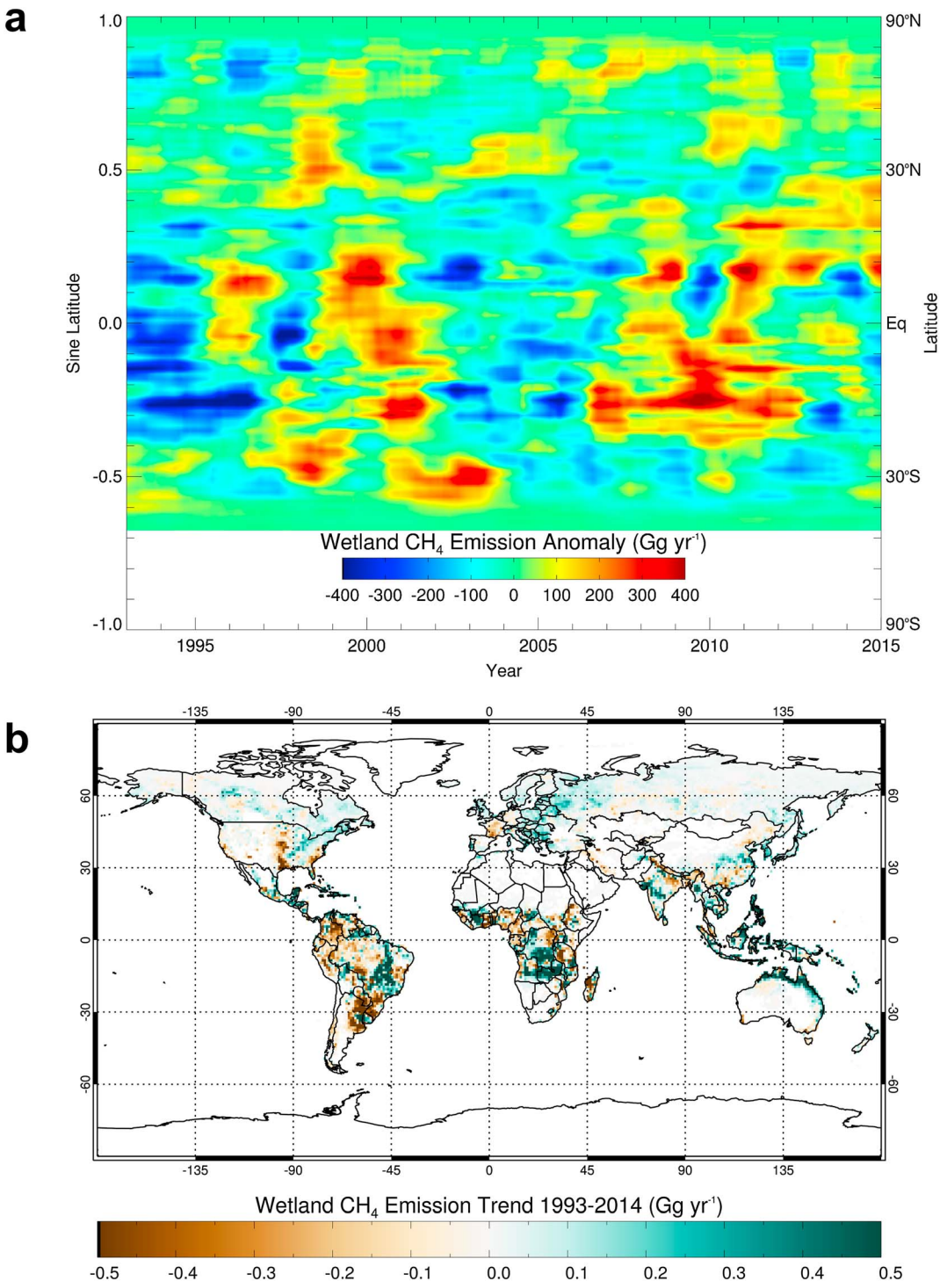

Figure 2. (a) Latitude-time plot of monthly JU wetland CH_4 emission anomalies (Gg/yr) between 1993 and 2014 binned into 1° latitude bands. Monthly anomalies are the deviation from the mean emission of the latitude band between 1993 and 2014. Note: *y* axis plotted as sine of latitude to equally weight surface area. (b) Spatial pattern of trends in 1° × 1° wetland CH_4 emissions (Gg/yr) from JU between 1993 and 2014.

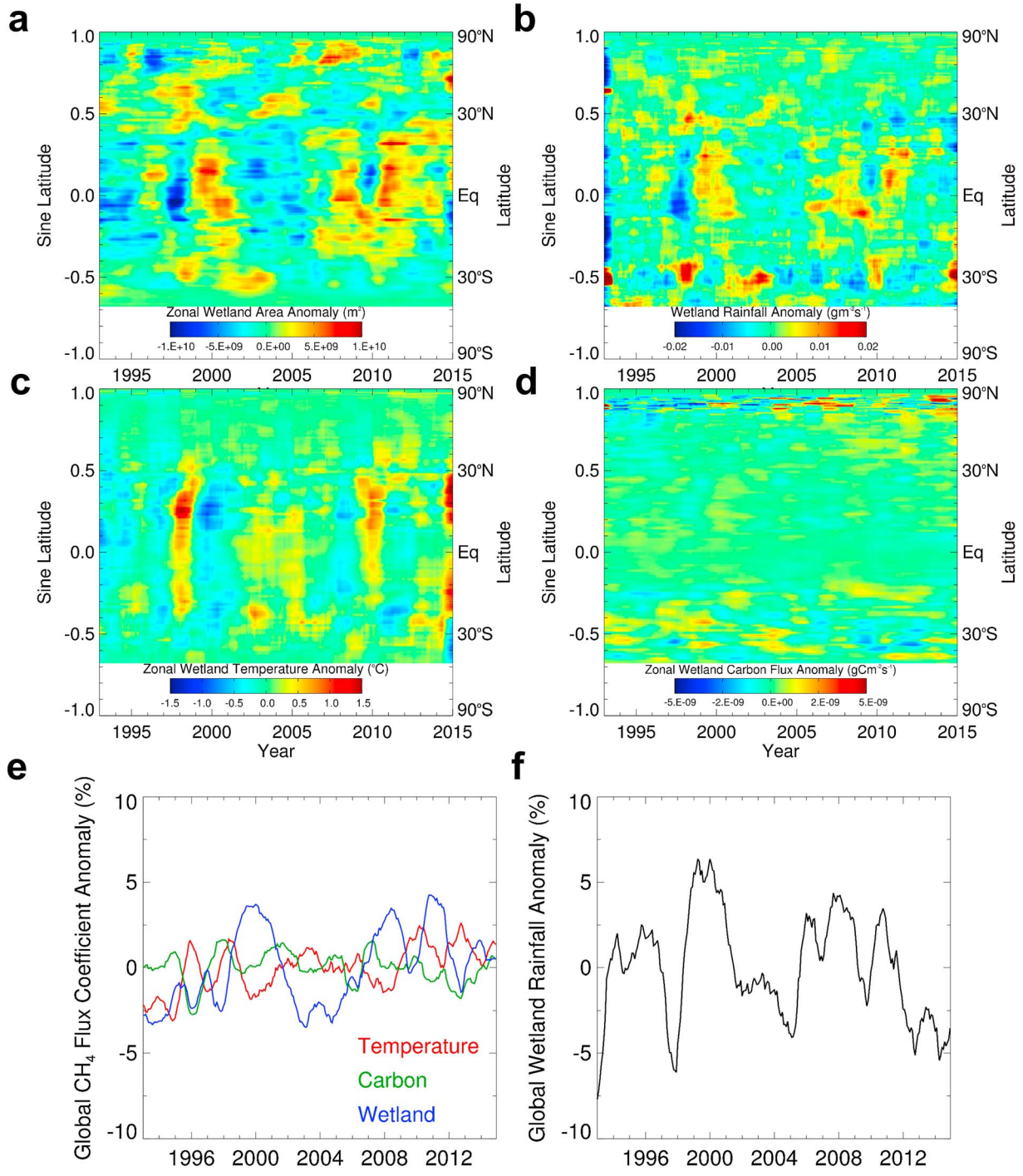

Figure 3. (a) Latitude-time plot of wetland area anomalies produced by JULES (m^2) between 1993 and 2014 binned into 1° bands and smoothed over a 12 month period. Monthly anomalies are calculated as the deviation from the mean area of the latitude band. Note: *y* axis plotted as sine of latitude to equally weight surface area. (b) As Figure 3a but for rainfall anomalies ($gm^{-2}s^{-1}$) weighted by the JULES climatological wetland area, taken from WFDEI using GPCC and CRU corrected rainfall [*Harris et al.*, 2014; *Weedon et al.*, 2014]. (c) Similar to Figure 3a but for upper layer soil temperature (°C) weighted by wetland area, from JULES. (d) Similar to Figure 3a but for the temperature-independent substrate carbon ($gCm^{-2}s^{-1}$) weighted by wetland area from JULES. (e) Global monthly wetland fraction (f_w, blue), temperature (f_{tem}, red), and substrate flux (f_{sub}, green) coefficient anomalies (%) weighted by wetland area between 1993 and 2014 and smoothed over a 12 month period. Note that the wetland area weighting varies with time; therefore, some temperature and substrate flux anomalies occur as a result of the variability in wetland area. (f) Global monthly rainfall anomaly (%) over the JULES climatological wetland area, taken from WFDEI using GPCC and CRU-corrected rainfall [*Harris et al.*, 2014; *Weedon et al.*, 2014], smoothed over a 12 month period.

The temperature and substrate coefficients were then weighted by grid cell wetland fraction and grid cell area to provide a global coefficient, from which monthly anomalies were calculated.

Globally, there is a statistically significant (95% level) positive trend in the wetland area CH_4 flux coefficient (f_{wet}) of 0.16%/yr over the 1993–2014 period (Figure 3e). There is a negative trend in rainfall over the model climatological wetland area, although this is not statistically significant (p value = 0.09) (Figure 3f). The trend in temperature flux coefficient (f_{tem}) anomaly is positive (0.13%/yr) and statistically significant. This trend causes high-latitude thawing, which controls the long-term trend in wetland area. The carbon substrate flux coefficient (f_{sub}) anomaly trend is slightly negative (−0.02%/yr) but is not statistically significant. Both the modeled CH_4 emission trend (1993–2014) and the interannual flux variability are dominated by changes in wetland area and temperature with small contributions from substrate, which is consistent with previous findings [e.g., *Ringeval et al*., 2010]. The reduction in our modeled wetland emissions from 2002 to 2006 is the result of a decrease in wetland area (f_{wet}: −2.0%), while the increase since 2007 is mainly the result of increases in wetland area (f_{wet}: +1.6%) and also temperature (f_{tem}: +0.7%).

Figure 4 compares TOMCAT predictions with atmospheric XCH_4 retrievals. Comparisons of GOSAT with the TOMCAT-JU simulation correlate slightly better ($\overline{R}$: 0.91) than with TOMCAT-BL ($\overline{R}$: 0.90) and TOMCAT-CL ($\overline{R}$: 0.90) for the TransCom regions. There is a slight interhemispheric offset between both model simulations and GOSAT; the three northern high-latitude regions have a mean concentration over the entire period of 1803.4 ppb in TOMCAT-JU, 1808.9 ppb in TOMCAT-BL, 1800.7 in TOMCAT-CL, and 1794.2 ppb in GOSAT. Through comparison of simulated and observed atmospheric SF_6 concentrations, *Wilson et al*. [2014] showed that interhemispheric transport in TOMCAT is somewhat too slow [see also *Patra et al*., 2011]. This causes TOMCAT to slightly overestimate (underestimate) Northern (Southern) Hemisphere CH_4 concentrations. The correlation, mean bias, and root-mean-square error (RMSE) values taken from comparisons show that TOMCAT-JU produces better agreement with GOSAT (R = 0.88, mean bias = 11.1 ppb, and RMSE = 7.7 ppb), compared to TOMCAT-BL (R = 0.84, mean bias = 13.4 ppb, and RMSE = 8.9 ppb) and TOMCAT-CL (R = 0.87, mean bias = 11.2, and RMSE = 7.7 ppb) (Figure 4b). Assuming that the model nonwetland CH_4 emissions are realistic, this suggests that JU captures both the seasonality and the interannual variability of wetland emissions well. It is important to note that JU emissions vary interannually over the entire time period, whereas BL only varies between 2003 and 2011. Comparisons with surface sites suggest JU produces a more accurate seasonal cycle than BL (see supporting information). Anthropogenic emissions are kept constant, and biomass burning emissions are slightly below average from 2010 to 2014, but the model still captures the continued CH_4 growth. These results would suggest that increases in wetland emissions in 2010 and 2011 contributed to growth post-2010, although high nonwetland emissions pre-2010 may still have contributed. Comparisons with flask measurements in Figure 4c show that the model reproduces the observed stalling and resumed growth of CH_4 between 1993 and 2014, although the modeled growth between 1999 and 2006 is larger than observed (TOMCAT-JU: 2.29 ppb/yr, TOMCAT-BL: 1.81 ppb/yr, TOMCAT-CL: 2.25 ppb/yr, and observations: 0.39 ppb/yr). This is mainly the result of an overestimation of the growth in 2006, which is due either to an underestimation of atmospheric OH [*McNorton et al*., 2016b] or an overestimation in emissions. A possible explanation for the overestimation is the high global biomass burning emissions estimated for 2006 (+34% compared to 1997–2014 mean). Comparisons with observations indicate that TOMCAT simulations provide a reasonable representation of atmospheric CH_4, although large uncertainties remain in atmospheric loss and nonwetland emission estimates. This suggests that JU emissions provide a reasonable representation of the spatial and interannual variability and are therefore suitable in the detection of wetland CH_4 trends. TOMCAT-JU (7.54 ppb/yr) captures most of the observed renewed growth post-2006 (8.12 ppb/yr), whereas TOMCAT-CL only captures some of the growth (6.48 ppb/yr), suggesting that increased wetland emissions have contributed an additional growth of approximately 1 ppb/yr (~13%) since 2007. The remaining growth is likely the result of nonwetland emissions and/or changes in atmospheric loss. The global CH_4 differences between TOMCAT_JU and TOMCAT_CL in Figure 4d show that the CH_4 concentration is 4 ppb higher by the end of 2014 when interannual variability in emissions is considered.

The model predicts variability in wetland CH_4 emissions, but the timescale of variability is not long enough to account for the entire slowdown in CH_4 growth (1999–2006). For 1999–2001 wetland emissions were high (3% above 1993–2014 average) so were unlikely to have contributed to the initial slowdown in growth. The continued stall in CH_4 growth (2002–2006) may have been caused by a 3% decrease in wetland

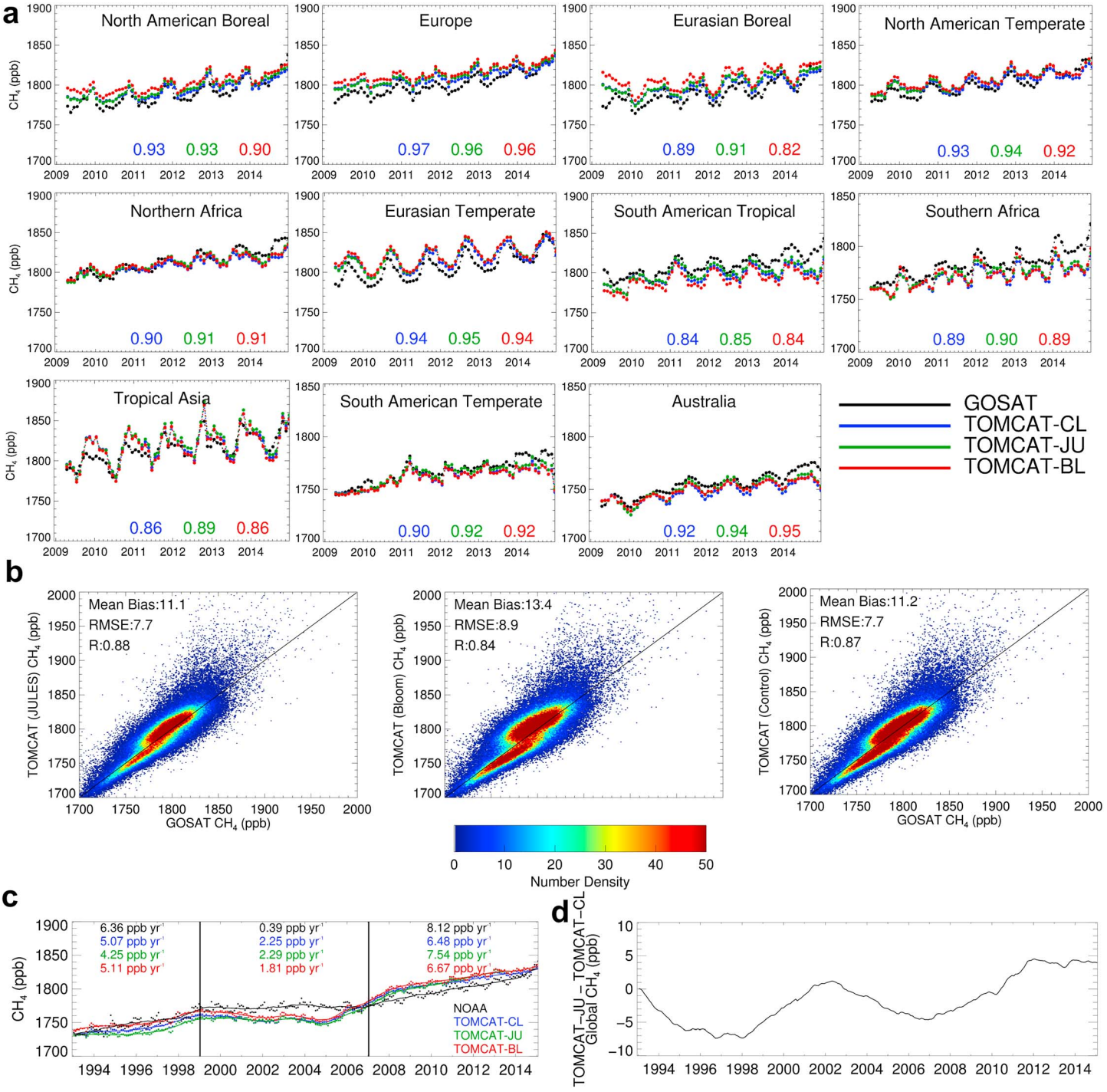

Figure 4. (a) Monthly mean XCH_4 concentrations (ppb) from GOSAT between April 2009 and December 2014 (black) for TransCom regions. Also shown are results from the three TOMCAT simulations with GOSAT averaging kernels applied, TOMCAT-CL (blue), TOMCAT-JU (green), and TOMCAT-BL (red). Correlation coefficients of model and observations are displayed. (b) Correlation of GOSAT XCH_4 with output from simulations TOMCAT-CL, TOMCAT-JU, and TOMCAT-BL (gridded into 1 ppb × 1 ppb bins) for months shown in Figure 4a. The color scale indicates the density of points. Also shown are the mean bias, RMSE, and correlation coefficient of each comparison. (c) Monthly (black circles) and deseasonalized global surface CH_4 (ppb) calculated from 19 NOAA sites (black) from 1993 to 2014. Also shown are results from CTM simulations TOMCAT-CL, TOMCAT-JU, and TOMCAT-BL. Numbers indicate average annual CH_4 growth (ppb/yr) for the periods 1993–1998, 1999–2006, and 2007–2014. (d) Difference in global CH_4 concentration (ppb) between TOMCAT_JU and TOMCAT_CL.

emissions, mainly from Australia (−9%), Northern Africa (−4%), and Tropical Asia (−4%). In 2007, when atmospheric CH_4 growth resumed, modeled emissions are again higher (177.6 Tg/yr) and remain high (2007–2014 average: 178.2 Tg/yr). The largest changes in emissions post-2006 occur in Southern Africa (+7%), Tropical Asia (+7%), and Australia (+18%). These results indicate that changes in wetland emissions contributed to the observed atmospheric CH_4 growth post-2006, in support of *Nisbet et al*. [2014].

4. Summary

Recent trends in global wetland CH_4 emissions from 1993 to 2014 were investigated using a substantially improved version of the JULES LSM. The modeled emissions, used within the TOMCAT CTM, gave a good representation ($R = 0.88$) of the spatial and temporal variability in atmospheric CH_4 when compared with satellite and surface data. However, it should be noted that there remain significant uncertainties in modeling the processes in wetland CH_4 emissions. The wetland emission model predicts a statistically significant positive trend (0.2%/yr) in emissions. This is mainly driven by a long-term positive temperature trend, which increases the methanogenesis rate and, by thawing frozen high-latitude regions, the wetland area. Interannual variability (±3%/yr, $\sigma = 4.8$ Tg) superimposed on the long-term trend is dominated by changes in precipitation over wetland regions. However, we find no evidence for a long-term trend in precipitation over wetland regions.

We find that the slowdown in global CH_4 growth rate from 1999 to 2006 was not caused by decreased wetland emissions. Furthermore, our model suggests that increased wetland emissions of 3% (relative to 1993–2006) contributed to the renewed global CH_4 growth since 2007.

The trends in atmospheric CH_4 growth are not exclusively a result of changes in wetland emissions. Over the period 1993–2014 anthropogenic emissions show large increases (~0.7%/yr) and the biomass burning emissions vary on an interannual basis, most noticeably during El Niño events. However, our study shows that even when accounting for those changes, the atmospheric loss and wetland emissions are keys to the interannual variability of CH_4 growth.

Acknowledgments

J.M. thanks NERC National Centre for Earth Observation (NCEO) for a studentship. C.W., M.P.C., and M.G. acknowledge support from NERC grants GAUGE (NE/K002244/1) and AMAZONICA (NE/F005806/1) and MOYA (NE/N015657/1). G.D.H. acknowledges support from the European Space Agency through its Support to Science Element initiative (ALANIS Methane), NCEO, and the NERC grants (MAMM, NE/I028327/1, and Tropical African Wetlands, NE/I01277X/2). R.J.P. is funded via an ESA Living Planet Fellowship with additional funding from NCEO. R.P. and H.B. acknowledge support from the ESA Greenhouse Gas Climate Change Initiative (GHG-CCI) and the NERC GAUGE and Amazonian Carbon Observatory Project. N.G. was supported by the Joint UK DECC/Defra Met Office Hadley Centre Climate Programme (GA01101). We thank the Japanese Aerospace Exploration Agency, National Institute for Environmental Studies, and the Ministry of Environment for the GOSAT data and their continued support as part of the Joint Research Agreement. We thank Anthony Bloom for supplying wetland CH_4 emissions. This research used the ALICE High Performance Computing Facility at the University of Leicester and the Arc1 facility at the University of Leeds. TCCON data were obtained from the TCCON Data Archive, hosted by the Carbon Dioxide Information Analysis Center (CDIAC) (tccon.onrl.gov). NOAA atmospheric CH_4 dry air mole fractions were obtained from the NOAA ESRL GMD Carbon Cycle Cooperative Global Air Sampling Network (esrl.noaa.gov). All model data used in this study are available through the University of Leeds ftp server; for access please contact j.r.mcnorton@leeds.ac.uk.

References

Bloom, A. A., P. I. Palmer, A. Fraser, and D. S. Reay (2012), Seasonal variability of tropical wetland CH_4 emissions: The role of the methanogen-available carbon pool, *Biogeosciences*, *9*, 2821–2830.

Bousquet, P., et al. (2006), Contribution of anthropogenic and natural sources to atmospheric methane variability, *Nature*, *443*, 439–443.

Bousquet, P., et al. (2011), Source attribution of the changes in atmospheric methane for 2006–2008, *Atmos. Chem. Phys.*, *11*, 3689–3700.

Chipperfield, M. (2006), New version of the TOMCAT/SLIMCAT off-line chemical transport model: Intercomparison of stratospheric tracer experiments, *Q. J. R. Meteorol. Soc.*, *132*, 1179–1203.

Christensen, T. R., A. Ekberg, L. Ström, M. Mastepanov, N. Panikov, M. Öquist, B. H. Svensson, H. Nykänen, P. J. Martikainen, and H. Oskarsson (2003), Factors controlling large scale variations in methane emissions from wetlands, *Geophys. Res. Lett.*, *30*(7), 1414, doi:10.1029/2002GL016848.

Ciais, P., C. Sabine, G. Bala, L. Bopp, V. Brovkin, J. Canadell, A. Chhabra, R. DeFries, J. Galloway, and M. Heimann (2014), Carbon and other biogeochemical cycles, in *Climate Change 2013: The Physical Science Basis. Contribution of Working Group I to the Fifth Assessment Report of the Intergovernmental Panel on Climate Change*, edited by T. F. Stocker et al., pp. 465–570, Cambridge Univ. Press, U. K., and New York.

Clark, D., L. Mercado, S. Sitch, C. Jones, N. Gedney, M. Best, M. Pryor, G. Rooney, R. Essery, and E. Blyth (2011), The joint UK land environment simulator (JULES), model description—Part 2: Carbon fluxes and vegetation, *Geosci. Model Dev.*, *4*, 701–722.

Coleman, K., and D. Jenkinson (1999), *A Model for the Turnover of Carbon in Soil Model Description and Windows Users Guide*, Rothamstead Research, Hertfordshire.

Cox, P. M. (2001), Description of the TRIFFID dynamic global vegetation model, Technical Note 24, Hadley Centre, United Kingdom Meteorological Office, Bracknell, U. K.

Dee, D., S. Uppala, A. Simmons, P. Berrisford, P. Poli, S. Kobayashi, U. Andrae, M. Balmaseda, G. Balsamo, and P. Bauer (2011), The ERA-Interim reanalysis: Configuration and performance of the data assimilation system, *Q. J. R. Meteorol. Soc.*, *137*, 553–597.

Dlugokencky, E. J., P. M. Lang, A. M. Crotwell, K. A. Masarie, and M. J. Crotwell (2015), Atmospheric methane dry air mole fractions from the NOAA ESRL carbon cycle cooperative global air sampling network, pp. 1983–2014, Version: 2015-08-03. [Available at ftp://aftp.cmdl.noaa.gov/data/trace_gases/ch4/flask/surface/.]

Fraser, A., P. Palmer, L. Feng, H. Boesch, A. Cogan, R. Parker, E. Dlugokencky, P. Fraser, P. Krummel, and R. Langenfelds (2013), Estimating regional methane surface fluxes: The relative importance of surface and GOSAT mole fraction measurements, *Atmos. Chem. Phys.*, *13*, 5697–5713.

Gauci, V., E. Matthews, N. Dise, B. Walter, D. Koch, G. Granberg, and M. Vile (2004), Sulfur pollution suppression of the wetland methane source in the 20th and 21st centuries, *Proc. Natl. Acad. Sci. U.S.A.*, *101*(34), 12,583–12,587.

Gedney, N., P. Cox, and C. Huntingford (2004), Climate feedback from wetland methane emissions, *Geophys. Res. Lett.*, *31*, L20503, doi:10.1029/2004GL020919.

Gurney, K. R., R. M. Law, A. S. Denning, P. J. Rayner, D. Baker, P. Bousquet, L. Bruhwiler, Y.-H. Chen, P. Ciais, and S. Fan (2002), Towards robust regional estimates of CO_2 sources and sinks using atmospheric transport models, *Nature*, *415*, 626–630.

Harris, I., P. Jones, T. Osborn, and D. Lister (2014), Updated high-resolution grids of monthly climatic observations—The CRU TS3. 10 Dataset, *Int. J. Climatol.*, *34*, 623–642.

Hayman, G., F. O'Connor, M. Dalvi, D. Clark, N. Gedney, C. Huntingford, C. Prigent, M. Buchwitz, O. Schneising, and J. Burrows (2014), Comparison of the HadGEM2 climate-chemistry model against in situ and SCIAMACHY atmospheric methane data, *Atmos. Chem. Phys.*, *14*, 13,257–13,280.

Huijnen, V., J. Williams, M. van Weele, T. van Noije, M. Krol, F. Dentener, A. Segers, S. Houweling, W. Peters, and J. de Laat (2010), The global chemistry transport model TM5: Description and evaluation of the tropospheric chemistry version 3.0, *Geosci. Model Dev.*, *3*, 445–473.

Jenkinson, D., S. Andrew, J. Lynch, M. Goss, and P. Tinker (1990), The turnover of organic carbon and nitrogen in soil [and discussion], *Philos. Trans. R. Soc. B.*, *329*, 361–368.

Kirschke, S., P. Bousquet, P. Ciais, M. Saunois, J. G. Canadell, E. J. Dlugokencky, P. Bergamaschi, D. Bergmann, D. R. Blake, and L. Bruhwiler (2013), Three decades of global methane sources and sinks, *Nat. Geosci.*, *6*, 813–823.

Kuze, A., H. Suto, M. Nakajima, and T. Hamazaki (2009), Thermal and near infrared sensor for carbon observation Fourier-transform spectrometer on the Greenhouse Gases Observing Satellite for greenhouse gases monitoring, *Appl. Optics*, *48*, 6716–6733.

Marthews, T., S. Dadson, B. Lehner, S. Abele, and N. Gedney (2015), High-resolution global topographic index values for use in large-scale hydrological modelling, *Hydrol. Earth Syst. Sci.*, *19*, 91–104.

Matthews, E., and I. Fung (1987), Methane emission from natural wetlands: Global distribution, area, and environmental characteristics of sources, *Global Biogeochem. Cycles*, *1*, 61–86, doi:10.1029/GB001i001p00061.

McNorton, J. (2016a), Analysis of recent atmospheric methane trends using models and observations, PhD thesis, Univ. of Leeds, U. K. [Available at http://etheses.whiterose.ac.uk/13294/.]

McNorton, J., et al. (2016b), Role of OH variability in the stalling of the global atmospheric CH_4 growth rate from 1999 to 2006, *Atmos. Chem. Phys.*, *16*, 7943–7956.

Melton, J. R., et al. (2013), Present state of global wetland extent and wetland methane modelling: Conclusions from a model inter-comparison project (WETCHIMP), *Biogeosciences*, *10*, 753–788.

Meng, L., R. Paudel, P. Hess, and N. Mahowald (2015), Seasonal and interannual variability in wetland methane emissions simulated by CLM4Me'and CAM-chem and comparisons to observations of concentrations, *Biogeosciences*, *12*, 4029–4049.

Monteil, G., S. Houweling, E. Dlugockenky, G. Maenhout, B. Vaughn, J. White, and T. Rockmann (2011), Interpreting methane variations in the past two decades using measurements of CH_4 mixing ratio and isotopic composition, *Atmos. Chem. Phys.*, *11*, 9141–9153.

Montzka, S. A., M. Krol, E. Dlugokencky, B. Hall, P. Jöckel, and J. Lelieveld (2011), Small interannual variability of global atmospheric hydroxyl, *Science*, *331*, 67–69.

Nisbet, E. G., E. J. Dlugokencky, and P. Bousquet (2014), Atmospheric science. Methane on the rise—Again, *Science*, *343*(6170), 493–495.

Olivier, J. G., J. A. Peters, and G. Janssens-Maenhout (2012), *Trends in Global CO2 Emissions 2012 Report*, PBL Netherlands Environmental Assessment Agency, Hague, Neth.

Parker, R., H. Boesch, A. Cogan, A. Fraser, L. Feng, P. I. Palmer, J. Messerschmidt, N. Deutscher, D. W. Griffith, and J. Notholt (2011), Methane observations from the Greenhouse Gases Observing SATellite: Comparison to ground-based TCCON data and model calculations, *Geophys. Res. Lett.*, *38*, L15807, doi:10.1029/2011GL047871.

Parker, R., H. Boesch, K. Byckling, A. J. Webb, P. I. Palmer, L. Feng, P. Bergamaschi, F. Chevallier, J. Notholt, and N. Deutscher (2015), Assessing 5 years of GOSAT Proxy XCH_4 data and associated uncertainties, *Atmos. Meas. Tech.*, *8*, 4785–4801.

Patra, P. K., S. Houweling, M. Krol, P. Bousquet, D. Belikov, D. Bergmann, H. Bian, P. Cameron-Smith, M. P. Chipperfield, and K. Corbin (2011), TransCom model simulations of CH_4 and related species: Linking transport, surface flux and chemical loss with CH_4 variability in the troposphere and lower stratosphere, *Atmos. Chem. Phys.*, *11*, 12,813–12,837.

Patra, P. K., T. Saeki, E. J. Dlugokencky, K. Ishijima, T. Umezawa, A. Ito, S. Aoki, S. Morimoto, E. A. Kort, and A. Crotwell (2016), Regional methane emission estimation based on observed atmospheric concentrations (2002–2012), *J. Meteorol. Soc. Jpn.*, *94*(1), 91–113.

Portmann, F. T., S. Siebert, and P. Döll (2010), MIRCA2000—Global monthly irrigated and rainfed crop areas around the year 2000: A new high-resolution data set for agricultural and hydrological modeling, *Global Biogeochem. Cycles*, *24*, GB1011, doi:10.1029/2008GB003435.

Prigent, C., F. Papa, F. Aires, C. Jimenez, W. B. Rossow, and E. Matthews (2012), Changes in land surface water dynamics since the 1990s and relation to population pressure, *Geophys. Res. Lett.*, *39*, L08403, doi:10.1029/2012GL051276.

Rigby, M., R. G. Prinn, P. J. Fraser, P. G. Simmonds, R. Langenfelds, J. Huang, D. M. Cunnold, L. P. Steele, P. B. Krummel, and R. F. Weiss (2008), Renewed growth of atmospheric methane, *Geophys. Res. Lett.*, *35*, L22805, doi:10.1029/2008GL036037.

Riley, W. J., Z. M. Subin, D. M. Lawrence, S. C. Swenson, M. S. Torn, L. Meng, N. M. Mahowald, and P. Hess (2011), Barriers to predicting changes in global terrestrial methane fluxes: Analyses using CLM4Me, a methane biogeochemistry model integrated in CESM, *Biogeosciences*, *8*, 1925–1953.

Ringeval, B., N. de Noblet-Ducoudré, P. Ciais, P. Bousquet, C. Prigent, F. Papa, and W. B. Rossow (2010), An attempt to quantify the impact of changes in wetland extent on methane emissions on the seasonal and interannual time scales, *Global Biogeochem. Cycles*, *24*, GB2003, doi:10.1029/2008GB003354.

Schaefer, H., S. E. M. Fletcher, C. Veidt, K. R. Lassey, G. W. Brailsford, T. M. Bromley, E. J. Dlugokencky, S. E. Michel, J. B. Miller, and I. Levin (2016), A 21st-century shift from fossil-fuel to biogenic methane emissions indicated by $^{13}CH_4$, *Science*, *352*, 80–84.

Segers, R. (1998), Methane production and methane consumption: A review of processes underlying wetland methane fluxes, *Biogeochemistry*, *41*, 23–51, doi:10.1023/A:10059290327643.

Spivakovsky, C., J. Logan, S. Montzka, Y. Balkanski, M. Foreman-Fowler, D. Jones, L. Horowitz, A. Fusco, C. Brenninkmeijer, and M. Prather (2000), Three-dimensional climatological distribution of tropospheric OH: Update and evaluation, *J. Geophys. Res.*, *105*, 8931–8980, doi:10.1029/1999JD901006.

Turnock, S., D. Spracklen, K. Carslaw, G. Mann, M. Woodhouse, P. Forster, J. Haywood, C. Johnson, M. Dalvi, and N. Bellouin (2015), Modelled and observed changes in aerosols and surface solar radiation over Europe between 1960 and 2009, *Atmos. Chem. Phys.*, *15*(16), 9477–9500.

van der Werf, G. R., J. T. Randerson, L. Giglio, G. Collatz, M. Mu, P. S. Kasibhatla, D. C. Morton, R. DeFries, Y. van Jin, and T. T. van Leeuwen (2010), Global fire emissions and the contribution of deforestation, savanna, forest, agricultural, and peat fires (1997–2009), *Atmos. Chem. Phys.*, *10*, 11,707–11,735.

Wania, R., I. Ross, and I. C. Prentice (2010), Implementation and evaluation of a new methane model within a dynamic global vegetation model: LPJ-WHyMe v1.3.1, *Geosci. Model Dev.*, *3*, 565–584.

Weedon, G. P., G. Balsamo, N. Bellouin, S. Gomes, M. J. Best, and P. Viterbo (2014), The WFDEI meteorological forcing data set: WATCH Forcing Data methodology applied to ERA-Interim reanalysis data, *Water Resour. Res.*, *50*, 7505–7514, doi:10.1002/2014WR015638.

Wilson, C., M. Chipperfield, M. Gloor, and F. Chevallier (2014), Development of a variational flux inversion system (INVICAT v1. 0) using the TOMCAT chemical transport model, *Geosci. Model Dev.*, *7*, 2485–2500.

Wunch, D., G. C. Toon, J.-F. L. Blavier, R. A. Washenfelder, J. Notholt, B. J. Connor, D. W. Griffith, V. Sherlock, and P. O. Wennberg (2011), The total carbon column observing network, *Philos. Trans. R. Soc. A.*, *369*, 2087–2112.

Yan, X., H. Akiyama, K. Yagi, and H. Akimoto (2009), Global estimations of the inventory and mitigation potential of methane emissions from rice cultivation conducted using the 2006 Intergovernmental Panel on Climate Change Guidelines, *Global Biogeochem. Cycles*, *23*, GB2002, doi:10.1029/2008GB003299.